MAPK/ERK signaling in gliomas modulates interferon responses, T cell recruitment, microglia phenotype, and immune checkpoint blockade efficacy

Kwang-Soo Kim[1,2†], Junyi Zhang[3,4,5,6†], Víctor A. Arrieta[1,2], Crismita Dmello[1,2], Elena Grabis[3,4,5,6], Karl Habashy[1,2], Joseph Duffy[1,2], Junfei Zhao[7,8], Andrew Gould[1,2], Li Chen[1,2], Jian Hu[9,10], Irina Balyasnikova[1,2], Dhan Chand[11], Dan Levey[11], Peter Canoll[12,13], Wenting Zhao[7,14], Peter A. Sims[7,14], Raul Rabadan[7,8], Surya Pandey[15], Bin Zhang[15], Catalina Lee-Chang[1,2*], Dieter Henrik Heiland[3,4,5,6*], and Adam M. Sonabend[1,2*]

[1]*Department of Neurological Surgery, Feinberg School of Medicine, Northwestern University, Chicago, IL, USA*
[2] *Northwestern Medicine Malnati Brain Tumor Institute of the Lurie Comprehensive Cancer Center, Feinberg School of Medicine, Northwestern University, Chicago, IL, USA*
[3]*Microenvironment and Immunology Research Laboratory, Medical Center - University of Freiburg, Freiburg, Germany*
[4]*Department of Neurosurgery, Medical Center - University of Freiburg, Freiburg, Germany*
[5]*Faculty of Medicine, University of Freiburg, Freiburg, Germany*
[6]*Translational NeuroOncology Research Group, Medical Center - University of Freiburg, Freiburg, Germany*
[7]*Department of Systems Biology, Columbia University, New York, NY, USA*
[8]*Department of Biomedical Informatics, Columbia University, New York, NY, USA*
[9]*Department of Cancer Biology, The University of Texas MD Anderson Cancer Center, Houston, TX, USA*
[10]*The University of Texas MD Anderson Cancer Center UTHealth Graduate School of Biomedical Sciences, Houston, TX, USA*
[11]*Agenus Inc., Lexington, MA, USA*
[12]*Herbert Irving Comprehensive Cancer Center, Columbia University Irving Medical Center, New York, NY, USA*
[13]*Department of Pathology and Cell Biology, Columbia University Irving Medical Center, New York, NY, USA*
[14]*Department of Biochemistry & Molecular Biophysics, Columbia University, New York, NY, USA*
[15]*Department of Hematology and Oncology, Northwestern University, Feinberg School of Medicine, Chicago, IL, USA*

[†]Equal contribution.

[*]Corresponding authors.

Catalina Lee-Chang PhD
catalina.leechang@northwestern.edu
Dieter Henrik Heiland MD
dieter.henrik.heiland@uniklinik-freiburg.de
Adam M. Sonabend MD
adam.sonabend@northwestern.edu

Abstract

Background. Glioblastoma (GB) remains a formidable challenge in neuro-oncology, with immune checkpoint blockade (ICB) showing limited efficacy in unselected patients. We previously recently established that MAPK/ERK signaling is associated with overall survival following anti-PD-1 and anti-CTLA-4 treatment in recurrent GB. However, the causal relationship between MAPK/ERK signaling and susceptibility to ICB, as well as the mechanisms underlying this association, remain poorly understood.

Method. We conducted *in vivo* kinome-wide CRISPR/Cas9 screenings in murine gliomas to identify key regulators of susceptibility to anti-PD-1 and $CD8^+$ T cell responses and performed survival studies to validate the most relevant genes. Additionally, paired single cell RNA-sequencing (scRNA-seq) with p-ERK staining, spatial transcriptomics on GB samples, and *ex-vivo* slice culture of a $BRAF^{V600E}$ mutant GB tumor treated with BRAFi/MEKi were used to determine the causal relationship between MAPK signaling, tumor cell immunogenicity, and modulation of microglia phenotype.

Results. CRISPR/Cas9 screens identified the MAPK pathway, particularly the RAF-MEK-ERK pathway, as the most critical modulator of glioma susceptibility to $CD8^+$ T cells, and anti-PD-1 across all kinases. Experimentally-induced ERK phosphorylation in gliomas enhanced survival with ICB treatment, led to durable anti-tumoral immunity upon re-challenge and memory T cell infiltration in long-term survivors. Elevated p-ERK in glioma cells correlated with increased interferon responses, antigen presentation and T cell infiltration in GB. Moreover, spatial transcriptomics and scRNA-seq analysis revealed the modulation of interferon responses by the MAPK/ERK pathway in $BRAF^{V600E}$ human GB cells with ERK1/2 knockout and in slice cultures of human $BRAF^{V600E}$ GB tissue. Notably, BRAFi/MEKi treatment disrupted the interaction between tumor cells and tumor-associated macrophages/microglia in slice cultures from $BRAF^{V600E}$ mutant GB.

Conclusion. Our data indicate that the MAPK/ERK pathway is a critical regulator of GB cell susceptibility to anti-tumoral immunity, modulating interferon responses, and antigen-presentation in glioma cells, as well as tumor cell interaction with microglia. These findings not only elucidate the mechanistic underpinnings of immunotherapy resistance in GB but also highlight the MAPK/ERK pathway as a promising target for enhancing immunotherapeutic efficacy in this challenging malignancy.

Introduction

Glioblastoma (GB), the most common and malignant primary brain tumors in adults, is characterized by pronounced genetic and molecular heterogeneity[1,2]. This diversity not only drives oncogene processes like cell proliferation but also leads to variations in the activation of key signaling pathways, such as MAPK and PI3K/AKT/mTOR[3,4]. The complexity of GB biology is further amplified by the numerous genetic and epigenetic alterations that can modulate these pathways, resulting in a spectrum of molecular profiles across tumors[5]. Moreover, the tumor microenvironment, plays a crucial role in GB progression, and in particular, tumor-associated macrophages and microglia (TAM) constitute up to 30-40% of the tumor volume[6]. These TAMs exhibit a phenotypic spectrum modulated by tumor cells, which varies across individual GB cases due to the underlying molecular heterogeneity[7]. This complex interplay between tumor cells and their microenvironment contributes significantly to the challenges in treating GB.

The molecular heterogeneity of GB significantly impacts clinical outcomes by contributing to the variability in treatment response[1,8-11]. In the context of immunotherapy, the variable tumor microenvironment likely contributes to inconsistent therapeutic outcomes[11]. Tailoring immunotherapy to account for the molecular diversity of GB could enhance efficacy in selected cases, even though traditional randomized controlled trials in unselected populations may not show overall survival benefits[12]. Anti-PD-1 (aPD-1) immunotherapy exemplifies this issue, as some cases demonstrate durable responses and prolonged survival, while multiple randomized controlled trials in unselected patients have failed to meet primary the efficacy endpoint[12-16].

We reported an association between mutations that activate MAPK pathway (*PTPN11*/*BRAF*) and GB susceptibility to aPD-1 therapy[10]. Notably, even in the absence of these mutations, MAPK activation, determined by the phosphorylation of the ERK protein (p-ERK), predicted overall survival in GB patients undergoing aPD-1 and anti-CTLA-4 (aCTLA-4) therapy across several independent cohorts[9,17]. Tumors with elevated p-ERK$^+$ tumor cell density exhibited a distinct microglial phenotype, characterized by the proximity of microglia to p-ERK$^+$ tumor cells and the expression of MHC class II antigen presenting molecules[9]. However, the causal relationship between MAPK signaling, this microglial phenotype, and the observed susceptibility to immunotherapy remains unsolved. Moreover, the mechanism by which tumor cells with active MAPK signaling become more immunogenic or modulate adjacent TAM are unclear.

96 In this study, we leveraged large *in vivo* CRISPR knockout (KO) screens, mouse glioma
97 models, *in vitro* experiments and reverse translation data derived from analyses of human tumors
98 to investigate the impact of tumor cell-intrinsic p-ERK and MAPK signaling on the tumor cell
99 immunogenicity, microglial phenotype and susceptibility to ICB. By elucidating the role of MAPK
100 signaling in shaping tumor immunogenicity and the microenvironment, our findings provide a
101 foundation for more precise and effective immunotherapy strategy tailored to the molecular profile
102 of glioblastoma.
103

Results

In vivo kinome-wide CRISPR/Cas9 screens identify MAPK/ERK signaling as a regulator for susceptibility to CD8$^+$ T cells and anti-PD-1 immunotherapy.

To investigate whether MAPK/ERK signaling contributes to immune cell recognition of glioma cells, we conducted kinome-wide CRISPR/Cas9 screens. GL261 glioma cells were transduced with a lentiviral sgRNA library resulting in the knockout (KO) of a single kinase gene per tumor cell. These transduced cells were then implanted intracranially into mice (Figure 1A). By comparing the implanted glioma cells into wildtype and *Cd8* KO mice, we identified kinase KO clones that were selected in the presence of CD8$^+$ T cells in the host[18]. Gene ontology (GO) analysis revealed the MAPK pathway as the most significantly enriched among all kinase pathways, in KO clones selected by CD8$^+$ T cells in wildtype mice, compared to *Cd8* KO hosts (Figure 1B). Among MAPK-related genes, *Map2k2* (encoding Mek2) and *Araf*, both upstream of Erk phosphorylation, showed the highest enrichment (Figure 1C and D).

To access whether these kinases, identified as critical for glioma recognition by CD8$^+$ T cells, also conferred susceptibility to ICB, we performed a similar CRISPR/Cas9 screen in which transduced glioma cells were implanted into wildtype mice treated with aPD-1 or with isotype control (IC) antibody. In this screen, the MAPK signaling pathway again emerged as the most enriched among all KO clones selected by aPD-1 treatment (Figure 1E). Within the MAPK pathway, genes such as *Araf*, *Raf1*, *Map2k1* (encoding Mek1), and *Mapk1* (encoding Erk2) showed the highest enrichment under aPD-1 treatment (Figure 1F and G), all involved in ERK activation. Consistent with previous reports, *Cd8* KO exhibited significantly reduced survival, while ICB treatment showed no survival difference in the GL261 mouse model (Supplementary Figure 1)[18,19]. Normalized sgRNA counts for each of these CRISPR screens are available in Supplementary Table 1.

MAPK activation enhances glioma susceptibility to aPD-1 therapy and promote durable anti-tumoral immunity.

To further investigate a causal link between MAPK signaling in glioma cells and anti-tumoral immunity, we overexpressed *Mek1* and *Mek2* in GL261 mouse glioma cells (GL261-Mek1/2), which led to increased Erk phosphorylation (GL261-Mek1/2 p-Erk^{high}; Figure 2A and B). Intracranial implantation of GL261-Mek1/2 p-Erk^{high} cells, resulted in tumors with higher CD8$^+$ T

135 cell infiltration compared to controls (Figure 2C), consistent with our earlier observation that KO
136 clones for *Mek1* and *Mek2*, were selected in the presence of $CD8^+$ T cells (Figure 1C and D).
137 Tumors derived from GL261-Mek1/2 p-Erk^{high} cells exhibited marked susceptibility to aPD-1
138 immunotherapy, with over 60% of the mice achieving long-term survival (P = 0.001, Figure 2D).
139 This effect was $CD8^+$ T cell-dependent, as *Cd8* KO hosts bearing GL261-Mek1/2 p-Erk^{high} tumors
140 showed no survival benefit from aPD-1 treatment (Figure 2E).

141 Interestingly, after multiple freeze-thaw cycles and several passages in culture, GL261-Mek1/2
142 cells maintained overexpression of *Mek1* and *Mek2* but lost ERK phosphorylation (Figure 2F).
143 When implanted intracranially, these cells with diminished p-Erk levels (GL261-Mek1/2 p-Erk^{low}),
144 showed reduced susceptibility to aPD-1 therapy, with no increase in median survival compared to
145 isotype control-treated mice, and only 22.2% of mice achieving long-term survival (Figure 2G),
146 further supporting the specific role of MAPK activation in immunotherapy response.

147 To further characterize the durability of anti-tumoral immunity, we re-challenged long-term
148 survivors with parental GL261 cells implanted on the contralateral side of the brain. Notably, four
149 out of six mice rejected the secondary tumors without any additional therapy (Figure 2H),
150 suggesting that the anti-tumoral immune response was related to MAPK activation and directed
151 against endogenous tumor antigens, rather than introduced transgenes. Immune phenotyping of
152 long-term survivors revealed increased CD8/CD4 T cell ratio (P = 0.0488), decreased intra-
153 tumoral $FoxP3^+$ regulatory T cells (Tregs) (P = 0.0050, Figure 2I), a higher ratio of central memory
154 to effector memory $CD8^+$ T cells (P = 0.0101) and reduced PD-1 expression on infiltrating $CD8^+$
155 T cells (Figure 2J).

156 We further validated these findings in a transgenic-derived murine glioma model QPP7, known
157 for its susceptibility to immunotherapy[20]. These cells exhibited elevated p-Erk levels and targeted
158 KO of Erk1 (QPP7-Erk1 KO) and Erk2 (QPP7-Erk2 KO) reduced the efficacy of aPD-1 therapy
159 compared to non-target controls (Supplementary Figure 2). Median survival difference between
160 IC-treated and aPD-1-treated groups was 7 days for QPP7-Erk1 KO (aPD-1: 64 days; IC: 57 days)
161 and 13 days for QPP7-Erk2 KO (aPD-1: 57 days and IC: 44 days) (Supplementary Figure 2). In
162 contrast, mice bearing QPP7-NTC tumors and treated with aPD-1 did not reach the median
163 survival endpoint, further supporting a potential role of MAPK/ERK signaling in immunotherapy
164 response (Supplementary Figure 2). Together, these data demonstrate that MAPK activation in

165 glioma cells enhances susceptibility to aPD-1 therapy and promotes durable, tumor-specific
166 immunity, primarily mediated by $CD8^+$ T cells.
167

168 **MAPK/ERK activation improves the efficacy of Fc-enhanced anti-CTLA-4 immune**
169 **checkpoint blockade in murine gliomas.**

170 Our CRISPR/Cas9 screens suggested that MAPK activation broadly impacts anti-tumoral
171 immunity in gliomas. To determine whether this effect extends beyond aPD-1 therapy, we
172 examined the impact of MAPK activation on the efficacy of aCTLA-4 immunotherapy. While
173 conventional aCTLA-4 therapy has not resulted in significant survival benefits for unselected GB
174 patients[16], our previous studies suggest that elevated tumor p-ERK levels could be a key
175 determinant of therapeutic response and prolonged survival in GB patients treated with a
176 combination of aPD-1 and aCTLA-4 blockade therapy[19,21].

177 To investigate whether MAPK activation also contributes to glioma susceptibility to aCTLA4
178 therapy, we used a mouse surrogate of botensilimab, a next generation Fc-enhanced aCTLA-4
179 antibody designed to bind with high affinity to activating Fcγ receptors expressed by host immune
180 cells and extend anti-tumor immunity against 'cold' tumors[22-24]. We recently reported that this
181 antibody is superior to conventional aCTLA-4 in glioma models[19], and is currently being evaluated
182 in an ongoing clinical trial in patients with GB (NCT05864534). In the GL261 mouse glioma
183 model, resistant to both conventional and Fc-enhanced aCTLA-4[19], activation of the MAPK
184 signaling led to improved efficacy of Fc-enhanced aCTLA-4 therapy. Mice bearing GL261
185 Mek1/2 p-ERK^{high} tumors treated with the Fc-enhanced aCTLA-4 antibody achieved a 100%
186 survival rate, which was significantly better than that observed in vector control tumors treated
187 with the same antibody ($P = 0.0291$), and to Mek1/2 p-ERK^{high} tumors treated with isotype control
188 antibody ($P = 0.0012$) (Figure 3). These findings highlight MAPK/ERK activation as a key
189 enhancer of glioma susceptibility to both aPD-1 and Fc-enhanced aCTLA-4 therapies, suggesting
190 a broader role in modulating tumor responsiveness to ICB therapy and its potential as a targeted
191 therapeutic strategy for glioblastoma.
192

193 **MAPK/ERK pathway is associated with glioblastoma cell response to Interferons.**

194 To elucidate the relationship between cell-intrinsic MAPK/ERK signaling and immune-related
195 tumor phenotypes in GB, we conducted a continuous paired analysis of scRNA-seq data from GB

patients with quantified p-ERK$^+$ cell density (Figure 4A). This analysis revealed correlations between p-ERK$^+$ cell density and gene expression of signaling pathways known to interact with MAPK/ERK, including receptor tyrosine kinase (RTK), WNT, AMP-activated protein kinase, and HIF-1α pathways (Supplementary Figure 3)[3,25-27]. Notably, both continuous and dichotomous analyses identified significant correlations between p-ERK$^+$ cell density and gene ontology (GO) themes associated with interferon (IFN) responses (Figure 4A and Supplementary Figure 3).

To validate the association of p-ERK with IFN responses at the cellular level, we employed multiplex immunofluorescence analysis. We compared the GB microenvironments between tumors with high (>3000 cells/mm^2) and low p-ERK density, staining for SOX2 to identify GB cells, p-ERK to indicate MAPK/ERK activity, and IRF9, a marker for IFN responses[28] (Figure 4B and C). IRF9 expression primarily localized to SOX2$^+$ tumor cells (Supplementary Figure 4). Notably, aligning with the transcriptomic results, SOX2$^+$IRF9$^+$ cells/mm^2 correlated with SOX2$^+$p-ERK$^+$ cells across tumors ($R = 0.62$, $P = 0.0104$). Tumors with high p-ERK exhibited a significantly higher density of SOX2$^+$p-ERK$^+$IRF9$^+$ tumor cells compared to low p-ERK tumors ($P = 0.0098$, Figure 4B and C).

To investigate the spatial relationship between ERK signaling, IFN responses, and T cell abundance, we analyzed spatially resolved multi-omic data, including gene expression and T cell receptor sequencing (SPTCR-seq), across 12 primary GB samples[29]. Spatial analysis revealed a correlation between the MAPK/ERK signaling pathway and type II IFN secretion, production, signaling (Figure 4D and E). Both type I and II IFN signatures were co-localized with regions of activated p-ERK signaling (Figure 4F). Consistent with our *Cd8* KO CRISPR/Cas9 screen (Figure 1B) and *in vivo* immunophenotype analysis (Figure 2C), p-ERK signaling was closely associated with T cell abundance, as determined by single-cell deconvolution and SPTCR-seq (Figure 4G). Further, analysis of public RNA-seq data from patients who received either adjuvant or neoadjuvant PD-1 blockade[14] suggested that high ERK signaling and corresponding type II IFN signaling were associated with improved survival (Supplementary Figure 5).

These findings collectively demonstrate a strong association between MAPK/ERK activation, interferon responses, and T cell infiltration in GB, providing mechanistic insights into the enhanced immunotherapy responsiveness observed in tumors with high MAPK/ERK activity.

MAPK/ERK pathway drives interferon responses in glioma.

227 To investigate the causal relationship between MAPK/ERK signaling and the observed tumor
228 cell phenotypes across tumors, RNA-seq data from AM38, a human GB cell line with $BRAF^{V600E}$
229 mutation, was analyzed following CRISPR-based single-gene KO of ERK1 and ERK2
230 (Supplementary Figure 6A). Given the strong association between the ERK pathway and cell
231 growth[30,31], ERK-deficient AM38 cells exhibited slower growth compared to non-target control
232 (NTC) AM38 cells (Supplementary Figure 6B).

233 Differential gene expression analysis comparing AM38-NTC with AM38-ERK1 KO and
234 AM38-ERK2 KO revealed GO themes modulated by MAPK/ERK signaling, including antigen
235 processing MHC class I, and IFN responses (Figure 5A and B). Gene set enrichment analysis
236 (GSEA) showed significant downregulation of type I and type II IFN responses genes in ERK1/2
237 KO cells, implicating ERK1/2 signaling in maintaining these immune-related tumor phenotypes
238 (Figure 5B).

239 Based on these findings, the potential for MAPK/ERK activation to enhance glioma cell
240 responsiveness to type I IFN was explored. Functional analysis of IFN-α responsiveness in AM38
241 cells revealed that ERK1/2 KO significantly reduced the upregulation of type I IFN response genes
242 (*IRF7*, *IRF9*, and *ISG15)*[32] following IFN-α exposure (Supplementary Figure 7A). Given our
243 previous observation that p-ERK in GB cells is associated with a distinct microenvironment
244 phenotype[9], the effect of ERK1/2 KO on cytokine secretion in response to IFN-α was further
245 examined. While AM38 secrete CCL3/4 and GM-CSF following IFN-α exposure, this secretion
246 was attenuated in AM38 ERK1 KO and ERK2 KO cells (Supplementary Figure 7B).

247 Analysis of a large public GB scRNA-seq dataset (GBmap)[33] revealed differential expression
248 of gene signatures derived from AM38-NTC and AM38-ERK1/2 KO across various cell
249 populations (Figure 5C). The AM38-NTC signature (associated with elevated p-ERK,
250 Supplementary Figure 6A) showed enhanced expression within tumor cells, particularly astrocyte
251 (AC)-like and neural progenitor cell (NPC)-like populations. Conversely, the AM38-ERK1/2 KO
252 signature was predominantly enriched in the mesenchymal (MES)-like cell population, whereas
253 IFN molecules, including IFN-α, IFN-β, and IFN-γ, are primarily expressed by T cells and myeloid
254 cells (Figure 5D).

255 To explore the causal relationship between MAPK/ERK signaling and these phenotypes in
256 human GB tissues, we utilized a novel autologous human neocortical slice model from a
257 $BRAF^{V600E}$ mutated GB patient (Supplementary Figure 8A)[34]. $BRAF^{V600E}$-mutated tumor cells

258 were implanted into cortex slices and treated with either temozolomide (TMZ) or BRAF/MEK
259 inhibitors (BRAFi/MEKi). The optimal BRAFi/MEKi combination was determined based on
260 maximal inhibition of tumor growth (Supplementary Figure 8B). Spatially resolved transcriptomic
261 and scRNA-seq analyses of the slices conducted 7 days after treatment (Figure 5F and G), revealed
262 downregulation of IFN signatures in BRAFi/MEKi-treated samples compared to TMZ treatment
263 (Figure 5H).
264
265 **MAPK/ERK signaling modulates antigen-presenting molecules in glioma cells.**
266 Earlier analysis of scRNA-seq data from GB specimens with high and low p-ERK levels
267 highlighted GO signatures related to antigen presentation (Figure 4A). Additionally, RNA-seq data
268 from AM38 cells with ERK1/2 KO indicated that MAPK/ERK signaling modulates transcriptional
269 signatures associated with antigen processing and presentation (Figure 5B). To determine whether
270 this p-ERK-associated phenotype is present in human GB, multiplex immunofluorescence was
271 used to assess the expression of antigen-presenting molecules. While HLA-DR was broadly
272 expressed across cell types (Supplementary Figure 9), the density of $SOX2^{+}HLA\text{-}DR^{+}p\text{-}ERK^{+}$
273 cells was significantly higher compared to $SOX2^{+}HLA\text{-}DR^{+}p\text{-}ERK^{-}$ cells ($P = 0.0011$, Figure 6A
274 and B).
275 The causal relationship between MAPK/ERK activation and antigen presenting machinery
276 expression in GB was further confirmed using the $BRAF^{V600E}$ GB slice culture model. Here,
277 scRNA-seq analysis revealed that BRAFi/MEKi treatment led to downregulation of HLA
278 molecules in glioma cells, compared to TMZ treatment or no treatment ($P = 1.42 \times 10^{-52}$, Figure
279 6C and D). Moreover, *in vitro* studies using AM38 cells showed that ERK2 KO specifically led to
280 downregulation of MHC II-related gene transcripts (Supplementary Figure 10A) and
281 corresponding protein levels (Supplementary Figure 10B). Similar findings were observed in the
282 murine glioma line QPP7, which exhibited elevated p-Erk, and susceptibility to aPD-1 therapy.
283 Both QPP7-Erk1 KO and QPP7-Erk2 KO showed downregulation these genes (Supplementary
284 Figure 10C and D).
285 These findings collectively demonstrate that MAPK/ERK signaling plays a crucial role in
286 modulating the expression of antigen presenting molecules in glioma cells, providing a
287 mechanistic link between MAPK activation and enhanced tumor cell immunogenicity.
288

MAPK signaling in tumor cells drives activation of tumor-associated microglia in GB.

Building on previous observations that high p-ERK gliomas exhibit a distinct microglia phenotype[9], the causal contribution of MAPK/ERK signaling to GB cell-microenvironment interactions was further investigated using the slice culture model of $BRAF^{V600E}$ GB. Graph-based cell proximity and communication analysis demonstrated that BRAFi/MEKi significantly reduced the communication between tumor cells and microglia. This effect was less pronounced for bone marrow-derived myeloid cells, indicating that MAPK signaling preferentialy contributes to cell-to-cell communication between tumor cells and tumor-infiltrating microglia (Figure 7A). Additionally, BRAFi/MEKi treatment modulated the microglial and TAM phenotypes. Notably, MAPK inhibition led to an increase in anti-inflammatory monocytes, and a decrease in proliferative microglia phenotype (Figure 7B). These findings demonstrate that MAPK /ERK signaling in GB cells plays a crucial role in shaping the tumor microenvironment, particularly in modulating microglia and TAM phenotypes and their interactions with tumor cells.

Material and Method

Orthotopic mouse glioma model. C57BL/6 mice were purchased from Charles River Laboratories and housed in a pathogen-free animal facility at Northwestern University Center for Comparative Medicine. All mouse work performed in this study were approved by the Institutional Animal Care and Use Committee (IACUC) under protocol number IS00014080. For tumor cell implantation, 6 to 8-week-old mice, were anesthetized with ketamine (100 mg/kg) and xylazine (10 mg/kg), and 100,000 glioma cells in 2.5 µl DPBS were injected intracranially at a specific brain coordinate after disinfecting and making a small cranial opening at 3 mm lateral and 2 mm caudal relative to the bregma using stereotaxic device (Harvard Apparatus). Post-surgery, animals were treated with isotype control or ICB antibodies and monitored until endpoints defined by the IACUC were met, including significant weight loss or severe neurological symptoms.

Cell culture. The mouse glioma cell lines GL261 was obtained from the National Institutes of Health and cultured in Dulbecco's modified Eagle's medium supplemented with 10% fetal bovine serum and 1% penicillin/streptomycin. QPP7 cells[20,35], kindly provided by Dr. Amy B. Heimberger from Northwestern University, were maintained in Dulbecco's modified Eagle's medium/F-12 (Gibco) supplemented with B-27 (Gibco), recombinant epidermal growth factor (EGF, 20 ng/ml, Peprotech), and recombinant basic fibroblast growth factor (bFGF, 20 ng/ml, Peprotech). All the cells were maintained in 5% CO_2 incubators at 37°C and tested for mycoplasma and confirmed negative before intracranial injection. Patient-derived GB cells after single cell suspension procedure were seeded in T-75 culture flasks and preserved in the cell culture incubator at 37 °C with 5% CO2 for recovery and following experiments. GM was used as cell culture medium for patient-derived GB cells in this study.

Kinome-wide CRISPR Cas9 Screening. Both CD8KO and anti-PD-1 kinome-wide CRISPR screens were analyzed using the Model-based Analysis of Genome-wide CRISPR-Cas9 Knockout (MAGeCK) computational tool.[36] Briefly, MAGeCK count command was used to map FASTq files to the sgRNAs in the Brie library. Counts were normalized to internal non-target sgRNA controls and gene essentiality scores (Beta-scores) was determined for each group relative to day 0 baseline controls using the MAGeCK maximum likelihood estimation (MLE) method.[37] Kyoto Encyclopedia of Genes and Genomes (KEGG) Pathway enrichment analysis was performed on significant genes (FDR < 0.05) in R (v4.2.3)[38] using clusterProfiler (v4.12.0)[39] package and plots were generated using enrichPlot (v1.24.0).[40]

335 **Immunophenotype analysis.** Tumor-bearing brans were processed immune profiling on 20 days
336 post intra-cranial tumor injection after 2 treatments. Following preparation of Percoll gradient
337 enriched single-cell suspension using a 70 μm cell strainer, cells underwent Fc blocking (TrueStain
338 FcX, Biolegend) for 10 min for further staining process. Cells then underwent surface staining
339 with primary antibodies and live/dead staining with Fixable Viability Dye eFluor 780
340 (eBioscience). After fixation and permeabilization (Foxp3/Transcription Factor Staining Buffer
341 Set, eBioscience), intracellular staining was performed. Antibodies used in this study were listed
342 in Supplementary Table 1. Flow cytometry data was acquired by the BD Symphony and analyzed
343 by FlowJo 10.8.1 (BD).
344 **Multiplex immunofluorescence staining.** The sections undergo deparaffinization with BOND
345 dewax solution and epitope retrieval process using a heat-induced method with BOND epitope
346 retrieval solution or pH9 EDTA buffer. DAB staining for immunohistochemistry was performed
347 to optimize antibody concentrations. The antibodies used in this analysis and the dilution factor
348 were depicted in Supplementary table 2. Multiple cycles of heat-induced epitope retrieval, protein
349 blocking, epitope labeling, and signal amplification were performed for multiplex staining, then
350 the slides were counterstained using spectral DAPI, finally mounted using Proling Diamond
351 Antifade Mountant (Thermo). Multispectral imaging was performed using the Vectra 3 Automated
352 Quantitative Pathology Imaging System (Akoya). Firstly, whole slide images were acquired, and
353 analyzed the tumor regions delineated by a certified neuropathologist at 20x of the original
354 magnification. First, whole slide images were acquired after autoadjusting focus and signal
355 intensity. Then, MSI was acquired in the tumor regions delineated by a certified neuropathologist
356 at 20x of the original magnification. For analysis of MSI, we created a spectral library for all Opal
357 dyes to subject acquired multispectral images to spectral unmixing that enabled the identification
358 and separation of weakly expressing and overlapping signals from background to visualize the
359 signal of each marker in inForm Tissue Finder software (inForm 2.6, Akoya Biosciences). Using
360 InForm, the adaptive cell segmentation feature was used to identify the nucleus of the analyzed
361 cells and to determine the nuclear and cytoplasmic compartments on each cell. A machine-learning
362 algorithm within inForm was used in which cells were automatically assigned to a specific
363 phenotype (GFAP+, TMEM119+, CD163+, CD16+, CD11c+, HLA-DR+). Batch analysis was
364 used to analyze all tumor samples under the same segmentation and phenotype settings. The
365 processing and analysis of images from all tumor samples were exported to cell segmentation

366 tables. Exported files from inForm were processed in R using R packages Phenoptr and
367 PhenoptrReports to merge and create consolidated single files for each tumor sample. Consolidated
368 files had cell phenotypes as outputs that we employed for further quantification and spatial
369 analyses using the Phenoptr R addin.

370 **RNA extraction and quantitative RT-PCR.** Total RNA was extracted from cells by manual
371 method using TRIzol (Invitrogen), and cDNA was synthesized from 1μg of total RNA using the
372 LeGene 1st Strand cDNA Synthesis System (Legene Biosciences) according to the manufacturer's
373 instructions. Quantitative PCR was performed using TOPrealTM qPCR 2X PreMIX (Bio-Rad)
374 and the CFX Connect Real-Time PCR Detection System (Bio-Rad). The primers used in this study
375 are summarized in Supplementary Table 2.

376 **Western Blot.** Cells were mixed with cell lysis buffer (Cell Signaling) containing protease and
377 phosphatase inhibitor cocktail (Thermo Fisher Scientific) and heated for 10min in 95 °C. Cell
378 lysates were resolved by sodium dodecyl sulfate-polyacrylamide gels, and separated proteins in
379 gel were transferred to polyvinylidene difluoride membranes (Bio-Rad). Membrane was blotted
380 with indicated antibody and immunoreactivity was detected with enhanced chemiluminescence
381 solution (Thermo Fisher Scientific). Antibodies used in this study were summarized in
382 Supplementary Table 3.

383 **Patient sample.** The ethics approval was issued by the local committee of the University of
384 Freiburg for data evaluation, imaging procedures and experimental design (Freiburg: protocol
385 100020/09 and 472/15_160880). All methods were carried out in accordance with the approved
386 guidelines, with written informed consent obtained from all subjects. The patient provided
387 preoperative (in the Department of Neurosurgery of the Medical Center - University of Freiburg,
388 Freiburg im Breisgau, Germany) informed consent to take part in the study. Therapeutically
389 resected access cortical tissue and glioblastoma tumor tissue were collected and transported to the
390 laboratory immediately after surgical resection.

391 **Human organotypic slice culture system.** Human organotypic slices were prepared and cultured
392 as we previously described. Therapeutically resected access cortical tissue was immediately
393 collected and immersed in the Preparation Medium saturated with carbogen (95% O_2 and 5% CO_2).
394 Damaged tissue was dissected away from the primary tissue block. The primary tissue block was
395 further dissected into smaller tissue blocks (6 x 6 mm^2 dimension) for tissue sectioning. Sectioning
396 was carried out using a Leica VT1200 semi-automatic vibratome (14912000001, Leica, Germany).

397 300 μm evenly thick cortical sections were collected in Growth Medium (GM) using a capillary
398 glass pipette and settled on ice for 10 minutes for recovery. Recovered slices were plated on
399 MilliporeTM inserts (PIPH03050, Merck KGaA, Germany) in 6-well plates (657160, Greiner
400 BIO-ONE, Germany) supplied with GM and further cultured in the incubator at 37°C with 5%
401 CO_2 for following experiments. A number of 3 sections per culture well is recommended. The first
402 medium refreshing was carried out 2 hours post tissue plating, followed by medium refreshing
403 every 48 hours as a regular basis throughout the culture period.
404 **Autologous GB cell suspension.** Patient-derived GB cell suspension was carried out, as we
405 previously described using a Neural Tissue Dissociation Kit (T) (130-093-231, Miltenyi Biotec,
406 Germany). Primary GB tissue obtained from the surgery was immediately processed and
407 dissociated with the Neural Tissue Dissociation Kit (T) in C-Tubes (130-093-237, Miltenyi Biotec,
408 Germany). Briefly, tissue was dissected into small pieces, incubated in enzyme 1 and enzyme 2
409 for 10 min with 2 min of tissue homogenizing in between each incubation. A filtering step followed
410 to remove all visible tissue pieces with pia matter. Single cells in the filtered supernatant was
411 further processed to remove myelin population along with red blood cells and non-viable cells.
412 Eventually, viable single patient-derived GB cells in the final supernatant was seeded into T-75
413 cell culture flasks for cell culture or directly snap-frozen in cryopreservation medium in -80°C.
414 **GB cell labeling and detection assay.** Cell TraceTM CFSE dye (C34570, ThermoFisher, USA)
415 was used in this study to label the autologous GB cells. Tumor cells from cell culture were washed
416 with PBS and detached with accutase for 5 min. CFSE dye was prepared with manufactor's
417 protocol. In a ratio of 1 μL dye per 2 x 10^6 cells, the CFSE dye was used to label the tumor cells.
418 Tumor cells were further observed under EVOS M7000 microscope (AMF7000, Thermofisher,
419 USA) coupled with its onstage incubator system (AMC1000, ThermoFisher, USA) to confirm the
420 success of fluorescent labeling for tumor cells.
421 **Personalized GB model.** Personalized GB model system was generated based on the autograft of
422 GB cells into the patient's cortical sections. The CFSE labeled tumor cells were resuspended and
423 inoculated into the patient's cortical sections using a Hamilton micro syringe (80330, Hamilton,
424 Switzerland) in the concentration of 20,000 cells per 1 μL.
425 **Tumor growth monitoring.** Fluorescent images of sections after inoculation were acquired using
426 EVOS M7000 microscope coupled with its onstage incubator system for monitoring tumor growth
427 on a time-resolved manner of every 24 hours till the end point of the culture experiment.

428 **Fluorescence associated cell sorting.** Fluorescence associated cell sorting (FACS) was performed
429 to screen targeted cell/nucleus populations. In brief, tissue was homogenized and nuclei were
430 isolated using Nuclei EZ Prep (NUC101-1KT, Merck KGaA, Germany) lysis buffer. Nuclei were
431 labeled using DAPI (32670#5MG, Merck KGaA, Germany). Myelin and debris were removed by
432 a sucrose gradient centrifugation step. 35,000 $DAPI^+$ events per condition were collected from
433 FACS sorter using 1.5 mL eppis coated with 100 µL 2% BSA.
434 **Single nucleus RNA-sequencing.** Single nucleus RNA-sequencing, a droplet based approach,
435 was performed according to the Chromium Next GEM Single Cell 3' v3.1 protocol from 10X
436 Genomics. Nuclei collected from FACS sorting were added to a prepared Master Mix and loaded
437 in Chromium Controller for RNA recovery and generating GEMs. After reverse transcription and
438 cDNA amplification, the enriched cDNA was fragmented, size-selected using SPRIselect (B23318,
439 Beckman Coulter, USA), indexed using i7 index, and SI primer was added. The average length of
440 final libraries was quantified using a 5200 Fragment Analyzer (M5310AA, Agilent, USA) with its
441 HS NGS Fragment kit (DNF-474, Agilent, USA) and the concentration was determined using
442 QubitTM 4 Fluorometer (Q33238, ThermoFisher, USA) with its 1x dsDNA HS kit (Q33231,
443 ThermoFisher, USA). Diluted, pooled, and denatured final library was loaded in Illumina NextSeq
444 550 Sequencing System. NextSeq High Output kit v2.5 (20024906, Illumina, USA) was used in
445 this study. Sequencing cycles for read1 – i7 – i5 – read2 were: 28 – 8 – 0 – 56.
446 **Spatially resolved transcriptomics.** 10 µm thick sections from fresh frozen tissue were mounted
447 on specially designed spatially barcoded Visium Gene Expression Slide (1000188, 10X Genomics,
448 Netherland). Mounted slide was fixed in 100% methanol following with H&E staining. EVOS
449 M7000 microscope coupled with 20x magnificence lens was used to acquire bright field images.
450 Post imaging processing was performed using FIJI ImageJ software. A permeabilization with pre-
451 optimized incubation time was further performed to maximize capture oligo binding with sample
452 mRNA. After reverse transcription, second strand cDNA was then cleaved off by denaturation.
453 Following with a qPCR quantification using KAPA SYBR FAST qPCR Master Mix (KK4600,
454 Roche, USA), cDNA was amplified and fragmented, and further size selected using SPRIselect.
455 Similar to single nucleus RNA-sequencing library preparation, cDNA library quality was
456 quantified using 5200 Fragment Analyzer., further indexed, amplified, and double-sided size
457 selected following with an average base pair length quantification using 5200 Fragment Analyzer
458 and a concentration quantification with Qubit^{TM} 4 Fluorometer. Final sequencing library was

generated after a dilution, normalization and denaturation step. Illumina NextSeq 550 Sequencing System coupled with its NextSeq High Output kit v2.5 (20024904, Illumina, USA) was used in this study. Sequencing cycles for read1 – i7 – i5 – read2 were set up as 28 – 10 – 10 – 102.

Statistical Analyses. Statistical analyses were performed using Prism Software 9.4.1 (GraphPad) and R Software 4.4.1 (R Studio). Unpaired Student's t-test was used to compare statistical differences between the two groups. For Kaplan-Meier survival curves, the log-rank (Mantel-Cox) test was adapted to determine the significance between groups. Statistical significances were presented in P-value, or $P < 0.05$ was considered significant, $*P < 0.05$, $**P < 0.01$, $***P < 0.001$, $****P < 0.0001$.

469 **Discussion**

470 Our study demonstrates the causal contribution of glioma-intrinsic MAPK/ERK signaling in
471 modulating anti-tumoral immunity and responsiveness to immunotherapy. Our findings provide
472 mechanistic insight into the previously observed association between MAPK-activating mutations,
473 elevated p-ERK levels, and improved survival in GB patients treated with aPD-1 and aCTLA-4
474 immune checkpoint blockade therapy[9,10,21]. While MAPK signaling is known for its oncogenic and
475 proliferative effects in cancer,[30] our results reveal its crucial role in shaping the tumor-immune
476 microenvironment, supporting the paradigm that molecular heterogeneity in GB tumors is linked
477 to the variability in the immune microenvironment, TAM phenotypes, and ultimately,
478 susceptibility to immunotherapy[11,41,42].

479 Our study provides several lines of evidence that MAPK activation in GB cells enhances $CD8^+$
480 T cell-mediated immune responses. Our CRISPR/Cas9 screen implicated the RAF-MEK-ERK
481 branch of the MAPK pathway in glioma susceptibility to T cell recognition. This finding is
482 corroborated by the differential responses to aPD-1 therapy in wildtype versus *Cd8* KO mice. The
483 distinct phenotype of $CD8^+$ T cells infiltrating the brains of long-term survivor mice with high p-
484 ERK tumors treated with aPD-1 further supports the role of these cells in the observed anti-tumor
485 immune response. Moreover, p-ERK promoted $CD8^+$ T cell infiltration in mouse gliomas, with
486 similar observations in human GB specimens. Consistent with this, clinical observations showed
487 robust brain/lesional T cell infiltration in patients with elevated p-ERK who responded to aPD-1
488 therapy[9]. Additionally, transgenic murine glioma models, demonstrated that gliomagenesis in *Cd8*
489 KO hosts, which lack $CD8^+$ T cells, leads to tumors with elevated p-ERK, that are also more
490 immunogenic[43].

491 The mechanism by which MAPK/ERK signaling enhances T cell recognition of GB cells and
492 response to immunotherapy appears to involve modulation of tumor cell immunogenicity and its
493 relationship with the tumor-infiltrating microenvironment, particularly microglia. Our findings
494 highlight the role of ERK phosphorylation in modulating both type I and type II IFN responses in
495 glioma cells consistent with previous literature implicating MAPK/ERK signaling in the IFN
496 response in other settings[31,44]. This regulation occurs through the activation of signaling pathways,
497 including STAT1 and the MAPK/ERK pathway, which together drive the expression of genes
498 involved in immune responses[45]. The mechanistic link between p-ERK and IFN responses in GB

499 is supported by evidence showing that inhibition of ERK signaling impairs the induction of IFN
500 response genes and dampens the overall immune response against tumors.

501 Furthermore, p-ERK was found to promote the expression of antigen presentation molecules
502 in GB cells and surrounding microglia, likely related to the IFN response driven by MAPK/ERK
503 signaling. This is consistent with antigen presentation being a downstream effect of IFN
504 signaling[46-48]. The increase in antigen presentation, favorable microglia phenotype driven by
505 MAPK/ERK signaling, as well as subsequent T cell infiltration and tumor recognition are
506 consistent with mechanisms known to contribute to effective tumor cell killing[9]. The immune-
507 modulating mechanisms driven by MAPK activation in GB cells translate into robust anti-tumoral
508 immune responses beyond aPD-1 blockade, as evidenced by enhanced susceptibility to aCTLA-4
509 therapy. This suggests that MAPK/ERK signaling may serve as a predictor of response to various
510 forms of GB immunotherapy and novel treatments that rely on T cell activity, such as vaccines,
511 CAR-T cells, BiTEs[49-51].

512 While MAPK activation contributes significantly to anti-tumoral immune responses, it appears
513 to be necessary but not sufficient to elicit robust tumor rejection. Indeed, not all GB patients with
514 elevated p-ERK benefit from aPD-1 therapy, whereas no patient with low p-ERK exhibited long
515 survival after ICB[9]. Other factors, including the presence of tumor-specific antigens, bone marrow-
516 derived immunosuppressive myeloid cells, T cell sequestration in the bone marrow, lymphopenia,
517 and the use of steroids may also play critical roles, and influence tumor susceptibility to ICB.
518 Additionally, several additional tumor-intrinsic features have been reported to modulate anti-
519 tumoral immunity[10,18].

520 While our study provides compelling evidence for the role of MAPK/ERK signaling in
521 modulating GB immunogenicity and immunotherapy response, several limitations should be
522 considered. Our experimental models, though informative, may not fully capture the complexity
523 of human GB. Likewise, while our $BRAF^{V600E}$ mutant GB slice culture model offers a unique
524 platform to study tumor-microenvironment interactions, it lacks the systemic immune components
525 and may not fully represent the *in vivo* tumor immune microenvironment. Additionally, while we
526 observed a correlation between p-ERK levels and immunotherapy response in patients, the limited
527 sample size necessitates validation through larger, prospective clinical studies across diverse
528 patient populations. Despite these limitations, our multi-modal approach, combining *in vitro*
529 studies, *in vivo* models, *ex vivo* human analyses, and large-scale omic approaches, provides a

530 framework for understanding the role of MAPK/ERK signaling in GB immunobiology. Future
531 studies addressing these limitations will be crucial for translating these findings into clinical
532 applications and potentially paving the way for more effective, personalized immunotherapies in
533 GB.

534 In conclusion, our study underscores the critical role of the RAF-MEK-ERK pathway in
535 regulating immune responses in GB, offering new insights into the molecular mechanisms that
536 drive immunotherapy responsiveness. By linking MAPK/ERK signaling to T cell-mediated tumor
537 recognition and response, these findings offer valuable insights into the heterogeneity of GB and
538 more importantly the potential of MAPK/ERK activation as a predictive biomarker and therapeutic
539 target. While these findings offer promising avenues for personalized immunotherapy in GB, they
540 also highlight the need for molecularly-guided approaches to address the heterogeneity of GB
541 treatment responses, paving the way for more effective, tailored strategies in this challenging
542 malignancy.
543

544 **Figure legends**

545 **Figure 1. *In vivo* kinome-wide CRISPR/Cas9 screens identify MAPK/ERK signaling as a**
546 **regulator for susceptibility to CD8$^+$ T cells and anti-PD-1 immunotherapy.** (A) Schematic
547 illustration of *in vivo* CRISPR/Cas9 screening. SgRNA library transduced to GL261 mouse glioma
548 cells and the cells were injected intracranially. Comparisons were 1) IC (n = 11) vs. aPD-1 (n =
549 12), 2) wildtype (n = 12) vs. *Cd8* KO mice (n = 20). (B) Gene enrichment analysis from the
550 CRISPR/Cas9 screenings comparing wildtype and *Cd8* KO mice. (C) Fold changes of sgRNAs
551 targeting MAPK/ERK pathway genes. Comparing wildtype and *Cd8* KO mice, 3 sgRNAs are
552 depicted. (D) Detailed diagrams of the MAPK signaling cascade, indicating log fold changes in
553 sgRNA enrichment. Log2(foldchange) was calculated based on the top performing sgRNA
554 depleted in *Cd8* KO mice. (E) Gene enrichment analysis from CRISPR/Cas9 screening comparing
555 mice received IC and aPD-1. (F) Fold changes of sgRNAs targeting MAPK/ERK pathway genes.
556 Comparing IC and aPD-1 group, 3 sgRNAs are depicted. (G) Diagrams of the MAPK signaling
557 cascade, indicating log fold changes in sgRNA enrichment. Log2(foldchange) was calculated
558 based on the top performing sgRNA enriched in aPD1 treated group. For B and E, the gene list of
559 the kinome was used as background (denominator) to calculate the gene ontology enrichment.

560 **Figure 2. MAPK/ERK activation in glioma cell contributes to susceptibility and durable**
561 **anti-tumoral immunity following anti-PD-1 therapy.** (A and B) Schematic illustration of cell
562 line generation and *in vivo* survival studies for GL261 Mek1/2 overexpression stable cell line was
563 established by lentiviral transduction and confirmed by Western blot to confer Erk1/2
564 phosphorylation. For treatment with ICB antibodies, treatment started 1 week after tumor
565 implantation and delivered intravenously 4 times every 3 or 4 days. (C) Flow cytometry based
566 immune cell infiltration analysis. After 20 days of tumor cell infusion, tumor infiltrating
567 lymphocytes were analyzed comparing control GL261 tumor (n = 5) and GL261-Mek1/2 p-Erk^{high}
568 tumor (n = 5). (D) Kaplan-Meier survival curve of GL261-CV (IC n = 10, aPD-1 n = 10) and
569 GL261-Mek1/2 p-Erk^{high} (IC, n = 6 and aPD-1, n = 9) treated with IC or aPD-1 antibody, conducted
570 in wildtype C57BL/6 mice. (E) Kaplan-Meier survival curve of control GL261-CV (IC, n = 4 and
571 aPD-1, n = 5) and GL261-Mek1/2 p-Erk^{high} (IC, n = 5 and aPD-1, n = 5) treated with IC or aPD-1
572 antibody, conducted in *Cd8* KO C57BL/6 mice. (F) Western blot analysis of Erk and Mek
573 phosphorylations and expressions after several passages and freeze/thaw cycles. The cell line was
574 referred as GL261-Mek1/2 p-Erk^{low}. (G) Kaplan-Meier survival curve of control GL261 tumor and

575 GL261-Mek1/2 p-Erk^{low} treated with IC (n = 9) or aPD-1 (n = 10), conducted in wildtype C57BL/6
576 mice. (H) The mice cohort from GL261-Mek1/2 p-Erk^{high}, the long-term survivors received
577 contralateral injection of wildtype GL261 cell infusion on day 120 post tumor cell injection
578 (control, n = 10 and long-term survivors, n = 6). (I) Immune landscape after 120 days of the
579 rechallenge. Comparing with brand-new tumor (CTL, n = 4), brains from long-term survivors
580 (LTS, n = 4) were analyzed for immune phenotyping. Flow cytometry data showing percoll-
581 enriched cells (left). Bar graph showing CD8$^+$ and CD4$^+$ T cell ratio (middle), Foxp3$^+$ cells in
582 CD4$^+$ T cell population (right). (I) Flow cytometry data showing expression of CD44 and CD62L
583 in CD8$^+$ T cells (left). Bar graph showing central memory T cell (CD44$^+$CD62L$^+$) to effector
584 memory T cell (CD44$^+$CD62L$^-$) ratio (middle). Flow cytometry data showing PD-1 expression in
585 CD8$^+$ T cells. The P values for survival studies were generated from low-rank test. Statistical
586 analysis for group comparison was done using unpaired two-tailed T test.

587 **Figure 3. Activation of MAPK/ERK pathway is associated with the efficacy of Fc-**
588 **enhanced anti-CTLA-4 therapy.** Kaplan-Meier survival curve of GL261-CV (IC, n = 9 and Fc-
589 enhanced aCTLA-4, n = 10) and GL261-Mek1/2 p-Erk^{high} (IC, n = 10 and Fc-enhanced aCTLA-
590 4, n = 10) treated with IC or Fc-enhanced aCTLA-4 antibody. For treatment with ICB antibodies,
591 treatment started 1 week after tumor implantation and delivered intravenously 4 times every 3 or
592 4 days. The P values were generated from low-rank test.

593 **Figure 4. MAPK/ERK pathway is associated with interferon signaling in GB.** (A)
594 Differentially expressed gene signatures of tumor cells from single cell RNA sequencing
595 comparing high and low p-ERK GB tumors. (B) Quantification analysis of immunofluorescence
596 analysis representing SOX2$^+$p-ERK$^+$IRF9$^+$ cell density in high p-ERK (n = 8) and low p-ERK (n
597 = 9) tumors. Unpaired two-tailed T test was used, and P-value is depicted. (C) Representative
598 immunohistochemistry (IHC) and immunofluorescence (IF) images of high p-ERK and low p-
599 ERK GB patients depicting p-ERK and IRF9 expression. Scale bar = 250 μm for IHC and 100 μm
600 for IF. (D) Example image of spatial multi-omic analysis of GB tumor representing p-ERK
601 signaling activity. (E) Spatial correlation analysis of GB tumors showing correlation between
602 MAPK and ERK1/2 signaling and type II IFN signatures. (F) Representative images of spatial
603 muli-omic analysis demonstrate Type I and II interferon responses in GB tumor. (G) Single-cell
604 composition after deconvolution representing the location of T cells and TAMs (upper). H&E

605 image demonstrates the histology of GB tumor, and the image of spatial T cell receptor sequencing
606 shows infiltrating T cells in GB tumor (low).

607 **Figure 5. MAPK/ERK pathway confers interferon responses in glioma.** (A) Bulk RNA-
608 seq analysis of human GB cell line AM38-NTC and AM38-ERK KO. Heatmap displaying
609 differential gene expression. NTC vs ERK1/2 KO is focused for further analysis. (B) Gene set
610 enrichment analysis comparing AM38-NTC and AM38-ERK1/2 KO. (C) Uniform manifold
611 approximation and projection dimensional reduction of the GBmap reference dataset. Each color
612 indicates the different cell types. (D) Gene signatures from AM38-NTC and ERK1/2 KO are
613 projected on GBmap reference dataset (top)[33]. Signatures of interferon alpha, beta, and gamma in
614 the GBmap reference dataset (bottom). (E) Spatial transcriptomic and scRNA-seq analysis of slice
615 culture of $BRAF^{V600E}$ GB tumor treated with BRAFi/MEKi. The H&E image demonstrates the
616 histology of slice culture (left). Each color indicates the different cell types (right). (F) Spatial
617 transcriptomic and single cell RNA sequencing analysis of slice culture GB samples treated with
618 temozolomide. (G) Spatial images of Type II interferon signature in slice culture samples treated
619 with temozolomide (left) and BRAFi/MEKi (right). (H) Differential analysis of interferon type I
620 and II signatures comparing temozolomide and BRAFi/MEKi treated slice culture.

621 **Figure 6. MAPK/ERK pathway modulates antigen presenting process in glioma cells.** (A)
622 Multiplex immunofluorescence analysis of human GB tumor. Representative images of high p-
623 ERK tumor (top) and low p-ERK tumor (bottom). Scale bar = 100 µm. (B) Quantified phenotypic
624 analysis of multiplex immunofluorescence across 16 GB patient samples. Bar graph showing
625 $SOX2^{+}HLA\text{-}DR^{+}$ cells comparing $p\text{-}ERK^{-}$ and $p\text{-}ERK^{+}$ cells. (C) Single cell analysis from slice
626 cultivated human GB tumor treated with temozolomide (left) and BRAFi/MEKi (right). (D)
627 Differential expression of human leukocyte antigen (HLA) in slice cultivated human GB sample
628 without treatment or temozolomide and BRAFi/MEKi treated (P = 1.42 x 10-52).

629 **Figure 7. MAPK activation in GB tumor is associated with interaction between tumor**
630 **cell and microglia.** (A) Cell-to-cell communication analysis of slice cultivated human GB samples
631 treated with temozolomide. (B) Phenotypic analysis of slice cultivated human GB samples treated
632 with BRAFi/MEKi.

633

634 **Author contributions:**

K.S. Kim, C. Lee-Chang, D.H. Heiland and A.M. Sonabend conceptualized the project. K.S. Kim, Junyi Zhang, D.H. Heiland and A.M. Sonabend drafted the manuscript. K. Habashy, A. Gould, D. Chand, D. Levey, I. Balyasnikova performed the majority of the editing of the manuscript. The experiments presented were conducted and analyzed by K.S. Kim, K. Habashy, A. Gould, V.A. Arrieta, C. Dmello. L. Chen. J. Zhang, E. Grabis, J. Duffy, J. Zhao, Wenting Zhao, P. Canoll, P. A. Sims, R. Rabadan, and D. H. Heiland performed the bioinformatic analysis. V.A. Arrieta, A.M. Sonabend, S. Pandey, and Bin Zhang performed the histological analysis of the human tumors. C. Lee-Chang, D.H. Heiland, and A.M. Sonabend supervised the study.

Acknowledgments and funding support: This work was supported by the NIH grants 1R01NS110703-01A1 (A.M.S., C.L.C.), 1U19CA264338-01 (A.M.S., C.L.C.), 1R01 NS122395 (I.V.B.), R37CA258426 (C.L.C), P50CA221747 SPORE for Translational Approaches to Brain Cancer (A.M.S., C.L.C., I.V.B.) and the Northwestern Nervous System Tumor Bank), as well as generous philanthropic support from the Sharon Moceri Foundation as well as Tina and Victor Kedaitis. R35CA253126 and Vagelos Precision Medicine Award (R.R. and J.Z.). Schematic illustrations are created with BioRender.com.

Disclosures: A.M. Sonabend has received in-kind and or funding support for research from Agenus, BMS, and CarThera. A.M. Sonabend, V.A. Arrieta, and R. Rabadan are co-authors of IP filed by Northwestern University related to the content of this manuscript. A.M. Sonabend is a paid consultant for Carthera and Enclear Therapies. P.A. Sims. receives patent royalties from Guardant Health

References

1. Neftel, C., Laffy, J., Filbin, M.G., Hara, T., Shore, M.E., Rahme, G.J., Richman, A.R., Silverbush, D., Shaw, M.L., Hebert, C.M., et al. (2019). An Integrative Model of Cellular States, Plasticity, and Genetics for Glioblastoma. Cell *178*, 835-849 e821. 10.1016/j.cell.2019.06.024.
2. Wang, Q., Hu, B., Hu, X., Kim, H., Squatrito, M., Scarpace, L., deCarvalho, A.C., Lyu, S., Li, P., Li, Y., et al. (2017). Tumor Evolution of Glioma-Intrinsic Gene Expression Subtypes Associates with Immunological Changes in the Microenvironment. Cancer Cell *32*, 42-56 e46. 10.1016/j.ccell.2017.06.003.
3. Behrooz, A.B., Talaie, Z., Jusheghani, F., Los, M.J., Klonisch, T., and Ghavami, S. (2022). Wnt and PI3K/Akt/mTOR Survival Pathways as Therapeutic Targets in Glioblastoma. Int J Mol Sci *23*. ARTN 1353 10.3390/ijms23031353.
4. Oprita, A., Baloi, S.C., Staicu, G.A., Alexandru, O., Tache, D.E., Danoiu, S., Micu, E.S., and Sevastre, A.S. (2021). Updated Insights on EGFR Signaling Pathways in Glioma. Int J Mol Sci *22*. ARTN 587 10.3390/ijms22020587.
5. Pearson, J.R.D., and Regad, T. (2017). Targeting cellular pathways in glioblastoma multiforme. Signal Transduct Tar *2*. ARTN e17040 10.1038/sigtrans.2017.40.
6. Zhou, Y.X., Wang, Y.L., Chen, H.L., Xu, Y.Y., Luo, Y., Deng, Y.C., Zhang, J.M., and Shao, A.W. (2021). Immuno-oncology: are TAM receptors in glioblastoma friends or foes? Cell Commun Signal *19*. ARTN 11 10.1186/s12964-020-00694-8.
7. Morisse, M.C., Jouannet, S., Dominguez-Villar, M., Sanson, M., and Idbaih, A. (2018). Interactions between tumor-associated macrophages and tumor cells in glioblastoma: unraveling promising targeted therapies. Expert Rev Neurother *18*, 729-737. 10.1080/14737175.2018.1510321.
8. Parker, N.R., Khong, P., Parkinson, J.F., Howell, V.M., and Wheeler, H.R. (2015). Molecular heterogeneity in glioblastoma: potential clinical implications. Front Oncol *5*. ARTN 55 10.3389/fonc.2015.00055.
9. Arrieta, V.A., Chen, A.X., Kane, J.R., Kang, S.J., Kassab, C., Dmello, C., Zhao, J., Burdett, K.B., Upadhyayula, P.S., Lee-Chang, C., et al. (2021). ERK1/2 phosphorylation predicts survival following anti-PD-1 immunotherapy in recurrent glioblastoma. Nat Cancer *2*, 1372-1386. 10.1038/s43018-021-00260-2.
10. Zhao, J., Chen, A.X., Gartrell, R.D., Silverman, A.M., Aparicio, L., Chu, T., Bordbar, D., Shan, D., Samanamud, J., Mahajan, A., et al. (2019). Immune and genomic correlates of response to anti-PD-1 immunotherapy in glioblastoma. Nat Med *25*, 462-469. 10.1038/s41591-019-0349-y.
11. Arrieta, V.A., Dmello, C., McGrail, D.J., Brat, D.J., Lee-Chang, C., Heimberger, A.B., Chand, D., Stupp, R., and Sonabend, A.M. (2023). Immune checkpoint blockade in glioblastoma: from tumor heterogeneity to personalized treatment. J Clin Invest *133*. 10.1172/JCI163447.
12. Lim, M., Xia, Y., Bettegowda, C., and Weller, M. (2018). Current state of immunotherapy for glioblastoma. Nat Rev Clin Oncol *15*, 422-442. 10.1038/s41571-018-0003-5.
13. Reardon, D.A., Brandes, A.A., Omuro, A., Mulholland, P., Lim, M., Wick, A., Baehring, J., Ahluwalia, M.S., Roth, P., Bahr, O., et al. (2020). Effect of Nivolumab vs Bevacizumab in Patients With Recurrent Glioblastoma: The CheckMate 143 Phase 3 Randomized Clinical Trial. JAMA Oncol *6*, 1003-1010. 10.1001/jamaoncol.2020.1024.

14. Cloughesy, T.F., Mochizuki, A.Y., Orpilla, J.R., Hugo, W., Lee, A.H., Davidson, T.B., Wang, A.C., Ellingson, B.M., Rytlewski, J.A., Sanders, C.M., et al. (2019). Neoadjuvant anti-PD-1 immunotherapy promotes a survival benefit with intratumoral and systemic immune responses in recurrent glioblastoma. Nature Medicine *25*, 477-+. 10.1038/s41591-018-0337-7.
15. Omuro, A., Reardon, D.A., Sampson, J.H., Baehring, J., Sahebjam, S., Cloughesy, T.F., Chalamandaris, A.G., Potter, V., Butowski, N., and Lim, M. (2022). Nivolumab plus radiotherapy with or without temozolomide in newly diagnosed glioblastoma: Results from exploratory phase I cohorts of CheckMate 143. Neurooncol Adv *4*, vdac025. 10.1093/noajnl/vdac025.
16. Omuro, A., Vlahovic, G., Lim, M., Sahebjam, S., Baehring, J., Cloughesy, T., Voloschin, A., Ramkissoon, S.H., Ligon, K.L., Latek, R., et al. (2018). Nivolumab with or without ipilimumab in patients with recurrent glioblastoma: results from exploratory phase I cohorts of CheckMate 143. Neuro-Oncology *20*, 674-686. 10.1093/neuonc/nox208.
17. Arrieta, V.A., Duerinck, J., Burdett, K.B., Habashy, K.J., Geens, W., Gould, A., Schwarze, J.K., Dmello, C., Kim, K.S., Saganty, R., et al. (2023). ERK1/2 Phosphorylation Predicts Survival in Recurrent Glioblastoma Following Intracerebral and Adjuvant PD-1/CTLA-4 Immunotherapy: A REMARK-Guided Analysis. Clin Cancer Res. 10.1158/1078-0432.CCR-23-1889.
18. Dmello, C., Zhao, J., Chen, L., Gould, A., Castro, B., Arrieta, V.A., Zhang, D.Y., Kim, K.S., Kanojia, D., Zhang, P., et al. (2023). Checkpoint kinase 1/2 inhibition potentiates anti-tumoral immune response and sensitizes gliomas to immune checkpoint blockade. Nat Commun *14*, 1566. 10.1038/s41467-023-36878-2.
19. Kim, K.-S., Habashy, K., Gould, A., Zhao, J., Najem, H., Amidei, C., Saganty, R., Arrieta, V.A., Dmello, C., Chen, L., et al. (2024). Fc-enhanced anti-CTLA-4, anti-PD-1, doxorubicin, and ultrasound-mediated BBB opening: A novel combinatorial immunotherapy regimen for gliomas. Neuro Oncol *in press* (*in press*), in press. in press.
20. Chen, C.H., Chin, R.L., Hartley, G.P., Lea, S.T., Engel, B.J., Hsieh, C.E., Prasad, R., Roszik, J., Shingu, T., Lizee, G.A., et al. (2023). Novel Murine Glioblastoma Models That Reflect the Immunotherapy Resistance Profile of Human Disease. Neuro Oncol. 10.1093/neuonc/noad025.
21. Arrieta, V.A., Duerinck, J., Burdett, K.B., Habashy, K.J., Geens, W., Gould, A., Schwarze, J.K., Dmello, C., Kim, K.S., Saganty, R., et al. (2024). ERK1/2 Phosphorylation Predicts Survival in Recurrent Glioblastoma Following Intracerebral and Adjuvant PD-1/CTLA-4 Immunotherapy: A REMARK-guided Analysis. Clin Cancer Res *30*, 379-388. 10.1158/1078-0432.CCR-23-1889.
22. Delepine, C., Levey, D., Krishnan, S., Kim, K.S., Sonabend, A., Wilkens, M., Tanne, A., Garcia-Brocano, P., Galand, C., Han, H.Y., et al. (2022). Botensilimab, an Fc-Enhanced Ctla-4 Antibody, Enhances Innate and Adaptive Immune Activation to Promote Superior Anti-Tumor Immunity in Cold and I-O Refractory Tumors. J Immunother Cancer *10*, A490-A490. 10.1136/jitc-2022-SITC2022.0470.
23. Waight, J.D., Chand, D., Dietrich, S., Gombos, R., Horn, T., Gonzalez, A.M., Manrique, M., Swiech, L., Morin, B., Brittsan, C., et al. (2018). Selective FcgammaR Co-engagement on APCs Modulates the Activity of Therapeutic Antibodies Targeting T Cell Antigens. Cancer Cell *33*, 1033-1047 e1035. 10.1016/j.ccell.2018.05.005.

24. Chand, D., Savitsky, D.A., Krishnan, S., Mednick, G., Delepine, C., Garcia-Broncano, P., Soh, K.T., Wu, W., Wilkens, M.K., Udartseva, O., et al. (2024). Botensilimab, an Fc-enhanced anti-CTLA-4 antibody, is effective against tumors poorly responsive to conventional immunotherapy. Cancer Discov. 10.1158/2159-8290.CD-24-0190.
25. Qin, A., Musket, A., Musich, P.R., Schweitzer, J.B., and Xie, Q. (2021). Receptor tyrosine kinases as druggable targets in glioblastoma: Do signaling pathways matter? Neurooncol Adv *3*, vdab133. 10.1093/noajnl/vdab133.
26. Peglion, F., Capuana, L., Perfettini, I., Boucontet, L., Braithwaite, B., Colucci-Guyon, E., Quissac, E., Forsberg-Nilsson, K., Llense, F., and Etienne-Manneville, S. (2022). PTEN inhibits AMPK to control collective migration. Nat Commun *13*, 4528. 10.1038/s41467-022-31842-y.
27. Moon, E.J., Sonveaux, P., Porporato, P.E., Danhier, P., Gallez, B., Batinic-Haberle, I., Nien, Y.C., Schroeder, T., and Dewhirst, M.W. (2010). NADPH oxidase-mediated reactive oxygen species production activates hypoxia-inducible factor-1 (HIF-1) via the ERK pathway after hyperthermia treatment. Proc Natl Acad Sci U S A *107*, 20477-20482. 10.1073/pnas.1006646107.
28. Platanitis, E., Demiroz, D., Schneller, A., Fischer, K., Capelle, C., Hartl, M., Gossenreiter, T., Muller, M., Novatchkova, M., and Decker, T. (2019). A molecular switch from STAT2-IRF9 to ISGF3 underlies interferon-induced gene transcription. Nat Commun *10*, 2921. 10.1038/s41467-019-10970-y.
29. Benotmane, J.K., Kueckelhaus, J., Will, P., Zhang, J., Ravi, V.M., Joseph, K., Sankowski, R., Beck, J., Lee-Chang, C., Schnell, O., and Heiland, D.H. (2023). High-sensitive spatially resolved T cell receptor sequencing with SPTCR-seq. Nat Commun *14*, 7432. 10.1038/s41467-023-43201-6.
30. Barbosa, R., Acevedo, L.A., and Marmorstein, R. (2021). The MEK/ERK Network as a Therapeutic Target in Human Cancer. Mol Cancer Res *19*, 361-374. 10.1158/1541-7786.MCR-20-0687.
31. Kiyatkin, A., van Alderwerelt van Rosenburgh, I.K., Klein, D.E., and Lemmon, M.A. (2020). Kinetics of receptor tyrosine kinase activation define ERK signaling dynamics. Sci Signal *13*. 10.1126/scisignal.aaz5267.
32. Ivashkiv, L.B., and Donlin, L.T. (2014). Regulation of type I interferon responses. Nat Rev Immunol *14*, 36-49. 10.1038/nri3581.
33. Ruiz-Moreno, C., Salas, S.M., Samuelsson, E., Brandner, S., Kranendonk, M.E.G., Nilsson, M., and Stunnenberg, H.G. (2022). Harmonized single-cell landscape, intercellular crosstalk and tumor architecture of glioblastoma. bioRxiv, 2022.2008.2027.505439. 10.1101/2022.08.27.505439.
34. Kuliesiute, U., Joseph, K., Straehle, J., Madapusi Ravi, V., Kueckelhaus, J., Kada Benotmane, J., Zhang, J., Vlachos, A., Beck, J., Schnell, O., et al. (2023). Sialic acid metabolism orchestrates transcellular connectivity and signaling in glioblastoma. Neuro Oncol *25*, 1963-1975. 10.1093/neuonc/noad101.
35. Shingu, T., Ho, A.L., Yuan, L., Zhou, X., Dai, C., Zheng, S., Wang, Q., Zhong, Y., Chang, Q., Horner, J.W., et al. (2017). Qki deficiency maintains stemness of glioma stem cells in suboptimal environment by downregulating endolysosomal degradation. Nat Genet *49*, 75-86. 10.1038/ng.3711.
36. Li, W., Xu, H., Xiao, T., Cong, L., Love, M.I., Zhang, F., Irizarry, R.A., Liu, J.S., Brown, M., and Liu, X.S. (2014). MAGeCK enables robust identification of essential genes from

794 genome-scale CRISPR/Cas9 knockout screens. Genome Biol *15*, 554. 10.1186/s13059-
795 014-0554-4.
796 37. Li, W., Koster, J., Xu, H., Chen, C.H., Xiao, T., Liu, J.S., Brown, M., and Liu, X.S. (2015).
797 Quality control, modeling, and visualization of CRISPR screens with MAGeCK-VISPR.
798 Genome Biol *16*, 281. 10.1186/s13059-015-0843-6.
799 38. Team, R.C. (2024). R: A language and environment for statistical computing (R
800 Foundation for Statistical Computing).
801 39. Wu, T., Hu, E., Xu, S., Chen, M., Guo, P., Dai, Z., Feng, T., Zhou, L., Tang, W., Zhan, L.,
802 et al. (2021). clusterProfiler 4.0: A universal enrichment tool for interpreting omics data.
803 Innovation (Camb) *2*, 100141. 10.1016/j.xinn.2021.100141.
804 40. Guangchuang Yu, Q.-Y.H., Yanyan Wu, and Xijin Ge (2024). enrichplot: Visualization of
805 Functional Enrichment Result (Bioconductor).
806 41. Andersen, B.M., Faust Akl, C., Wheeler, M.A., Chiocca, E.A., Reardon, D.A., and
807 Quintana, F.J. (2021). Glial and myeloid heterogeneity in the brain tumour
808 microenvironment. Nat Rev Cancer *21*, 786-802. 10.1038/s41568-021-00397-3.
809 42. Chen, D., Varanasi, S.K., Hara, T., Traina, K., Sun, M., McDonald, B., Farsakoglu, Y.,
810 Clanton, J., Xu, S., Garcia-Rivera, L., et al. (2023). CTLA-4 blockade induces a microglia-
811 Th1 cell partnership that stimulates microglia phagocytosis and anti-tumor function in
812 glioblastoma. Immunity *56*, 2086-2104 e2088. 10.1016/j.immuni.2023.07.015.
813 43. Kane, J.R., Zhao, J., Tsujiuchi, T., Laffleur, B., Arrieta, V.A., Mahajan, A., Rao, G., Mela,
814 A., Dmello, C., Chen, L., et al. (2020). CD8(+) T-cell-Mediated Immunoediting Influences
815 Genomic Evolution and Immune Evasion in Murine Gliomas. Clin Cancer Res *26*, 4390-
816 4401. 10.1158/1078-0432.CCR-19-3104.
817 44. Mazewski, C., Perez, R.E., Fish, E.N., and Platanias, L.C. (2020). Type I Interferon (IFN)-
818 Regulated Activation of Canonical and Non-Canonical Signaling Pathways. Front
819 Immunol *11*, 606456. 10.3389/fimmu.2020.606456.
820 45. Banik, S., Rakshit, S., and Sarkar, K. (2021). The Role of STAT1 in T Helper Cell
821 Differentiation during Breast Cancer Progression. J Breast Cancer *24*, 253-265.
822 10.4048/jbc.2021.24.e34.
823 46. Frucht, D.M., Fukao, T., Bogdan, C., Schindler, H., O'Shea, J.J., and Koyasu, S. (2001).
824 IFN-gamma production by antigen-presenting cells: mechanisms emerge. Trends Immunol
825 *22*, 556-560. 10.1016/s1471-4906(01)02005-1.
826 47. Jhunjhunwala, S., Hammer, C., and Delamarre, L. (2021). Antigen presentation in cancer:
827 insights into tumour immunogenicity and immune evasion. Nat Rev Cancer *21*, 298-312.
828 10.1038/s41568-021-00339-z.
829 48. Duong, E., Fessenden, T.B., Lutz, E., Dinter, T., Yim, L., Blatt, S., Bhutkar, A., Wittrup,
830 K.D., and Spranger, S. (2022). Type I interferon activates MHC class I-dressed CD11b(+)
831 conventional dendritic cells to promote protective anti-tumor CD8(+) T cell immunity.
832 Immunity *55*, 308-323 e309. 10.1016/j.immuni.2021.10.020.
833 49. Singh, K., Hotchkiss, K.M., Mohan, A.A., Reedy, J.L., Sampson, J.H., and Khasraw, M.
834 (2021). For whom the T cells troll? Bispecific T-cell engagers in glioblastoma. J
835 Immunother Cancer *9*. 10.1136/jitc-2021-003679.
836 50. Bagley, S.J., Desai, A.S., Linette, G.P., June, C.H., and O'Rourke, D.M. (2018). CAR T-
837 cell therapy for glioblastoma: recent clinical advances and future challenges. Neuro Oncol
838 *20*, 1429-1438. 10.1093/neuonc/noy032.

839 51. Medikonda, R., Dunn, G., Rahman, M., Fecci, P., and Lim, M. (2021). A review of
840 glioblastoma immunotherapy. J Neurooncol *151*, 41-53. 10.1007/s11060-020-03448-1.
841

Figure 1. Kinome-wide CRISPR/Cas9 screenings identify MAPK/ERK signaling as a regulator for susceptibility to immune system in murine gliomas.

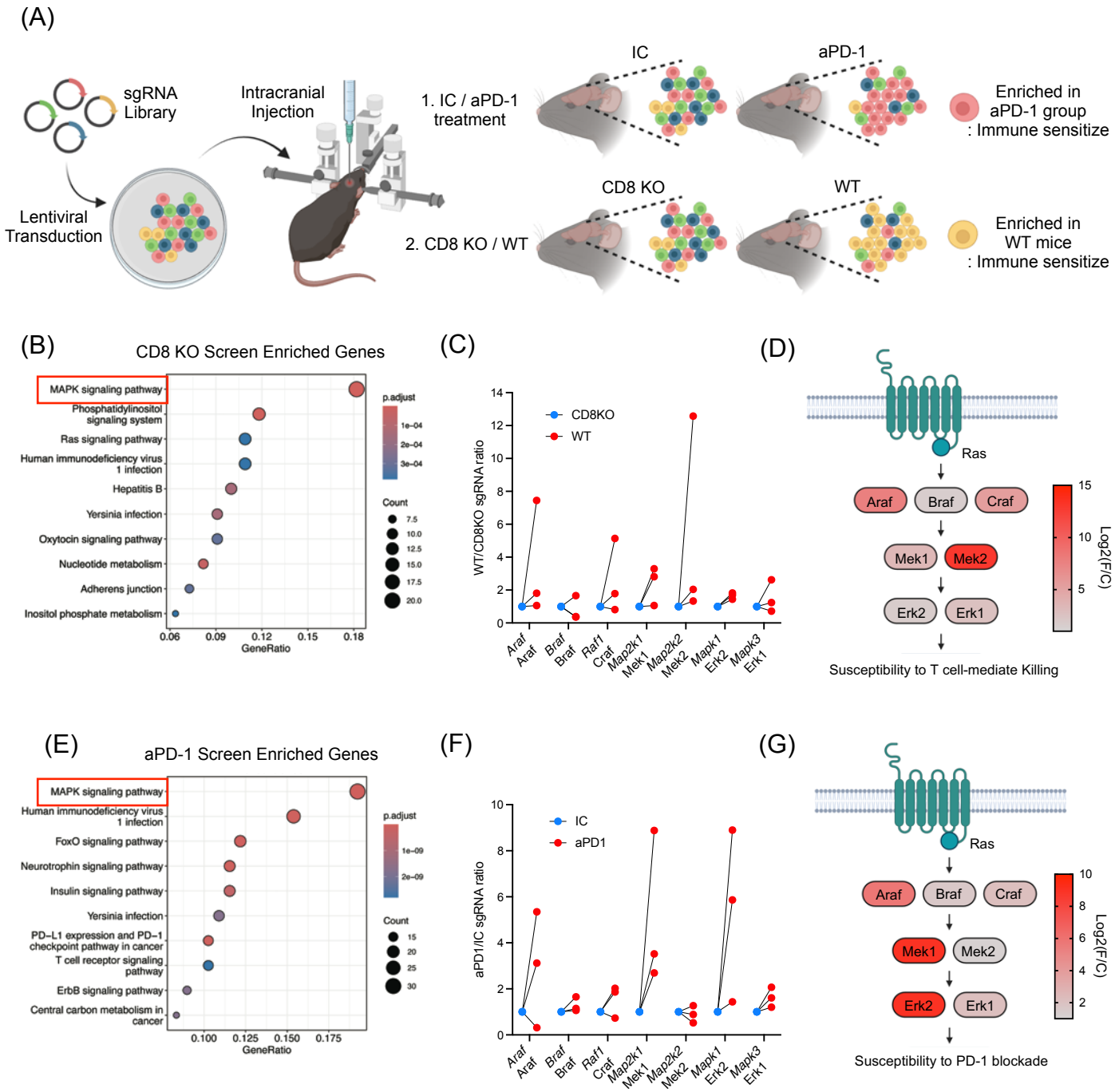

Figure 2. MAPK activation in glioma cell contributes to susceptibility and durable antitumoral immunity following anti-PD-1 therapy.

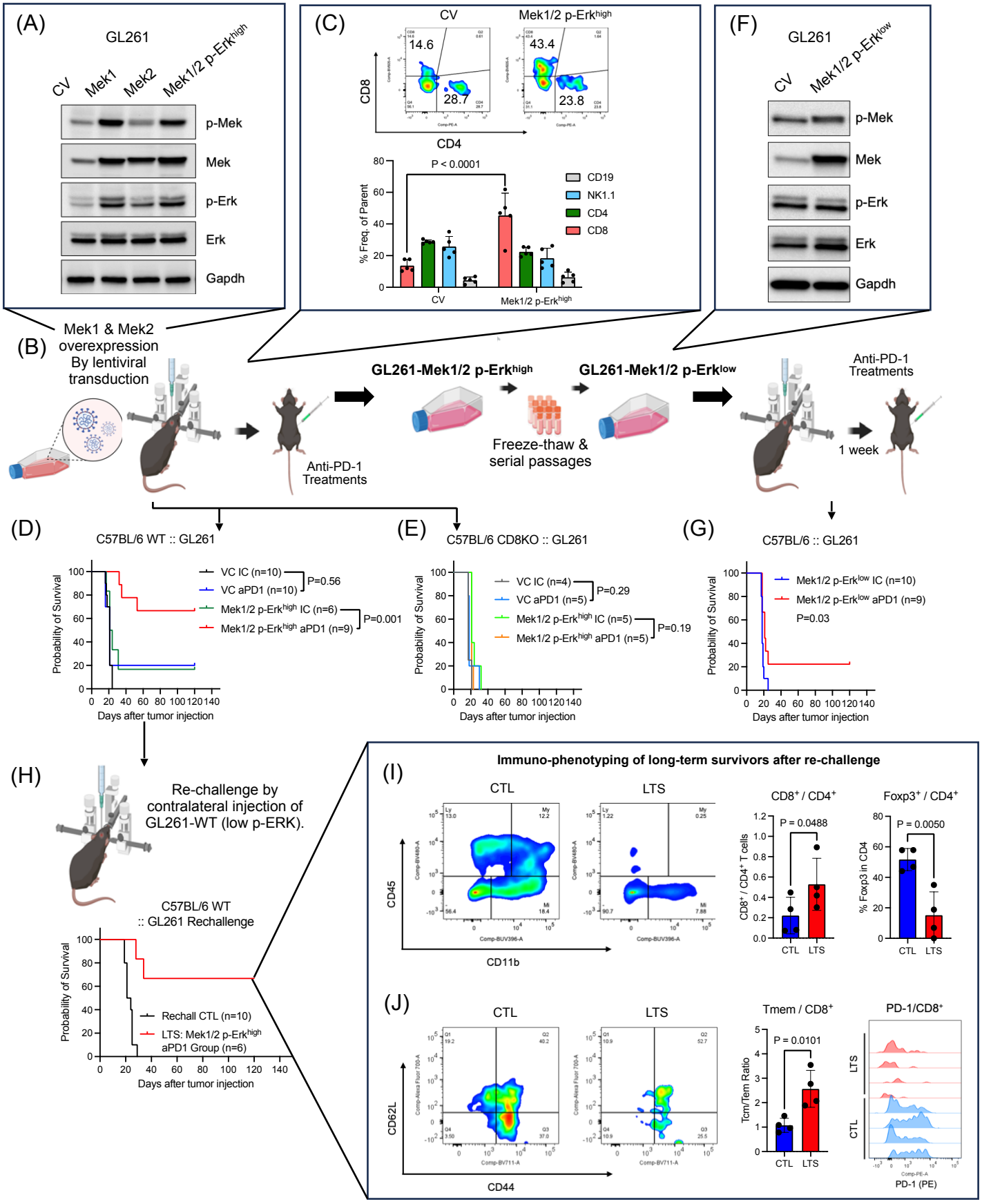

Figure 3. Activation of MAPK/ERK pathway is associated with the efficacy of Fc-enhanced anti-CTLA-4 therapy

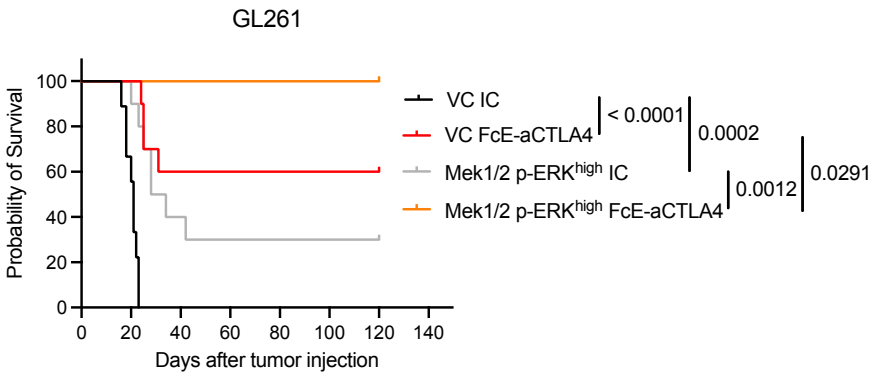

Figure 4. MAPK/ERK pathway is associated with interferon signaling in glioblastoma

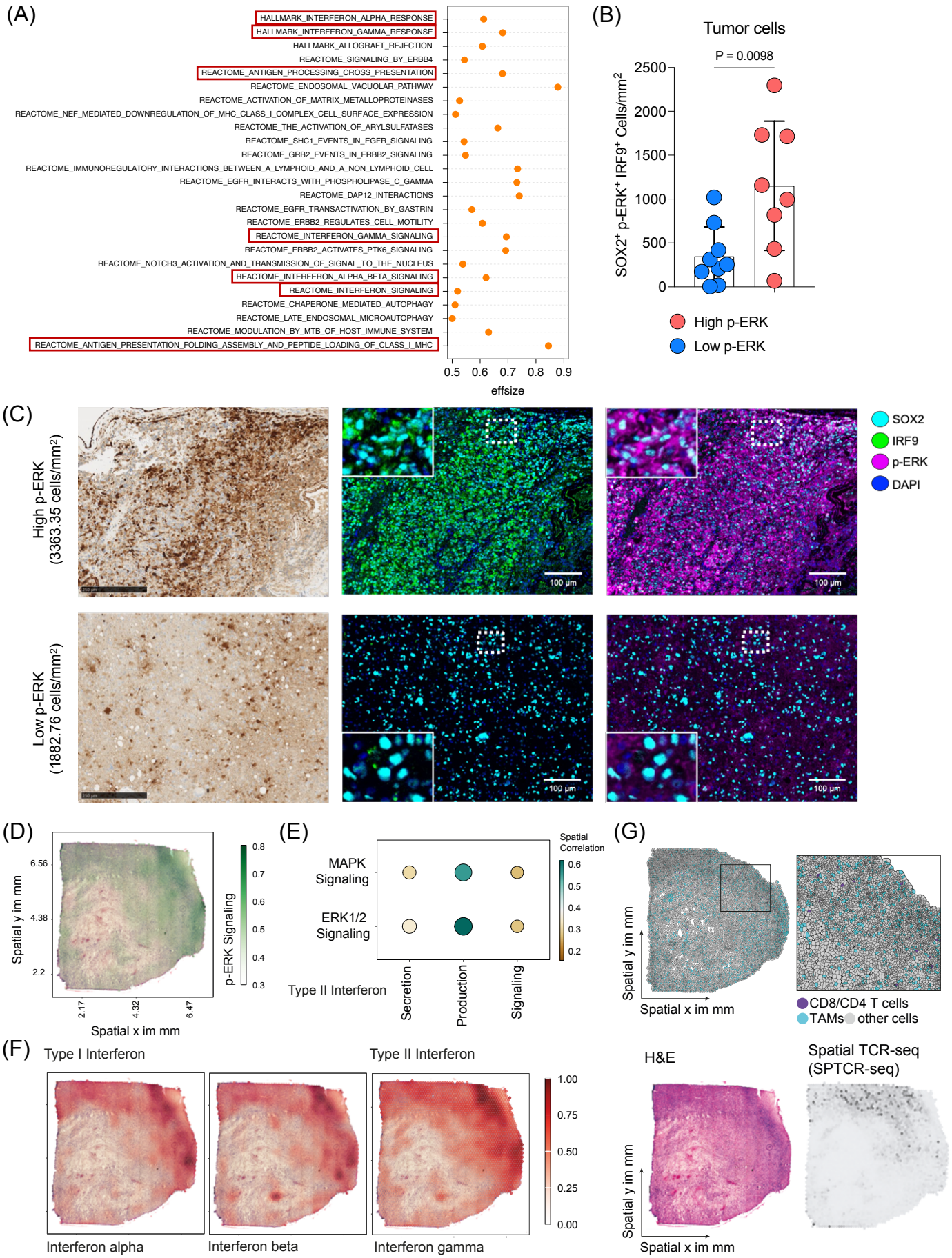

Figure 5. MAPK/ERK pathway confers interferon responses in glioma.

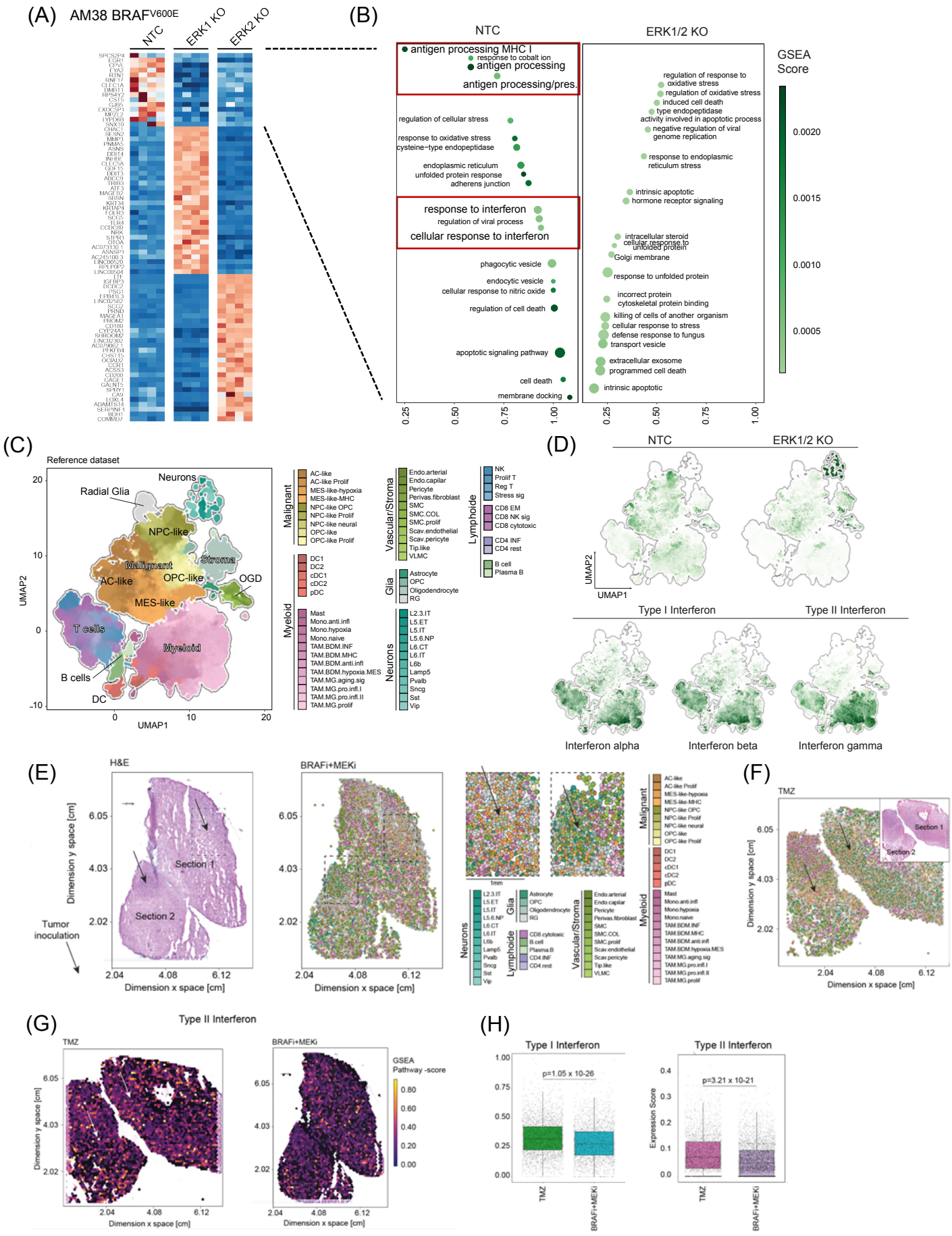

Figure 6. MAPK/ERK pathway modulates antigen presenting process in glioma cells.

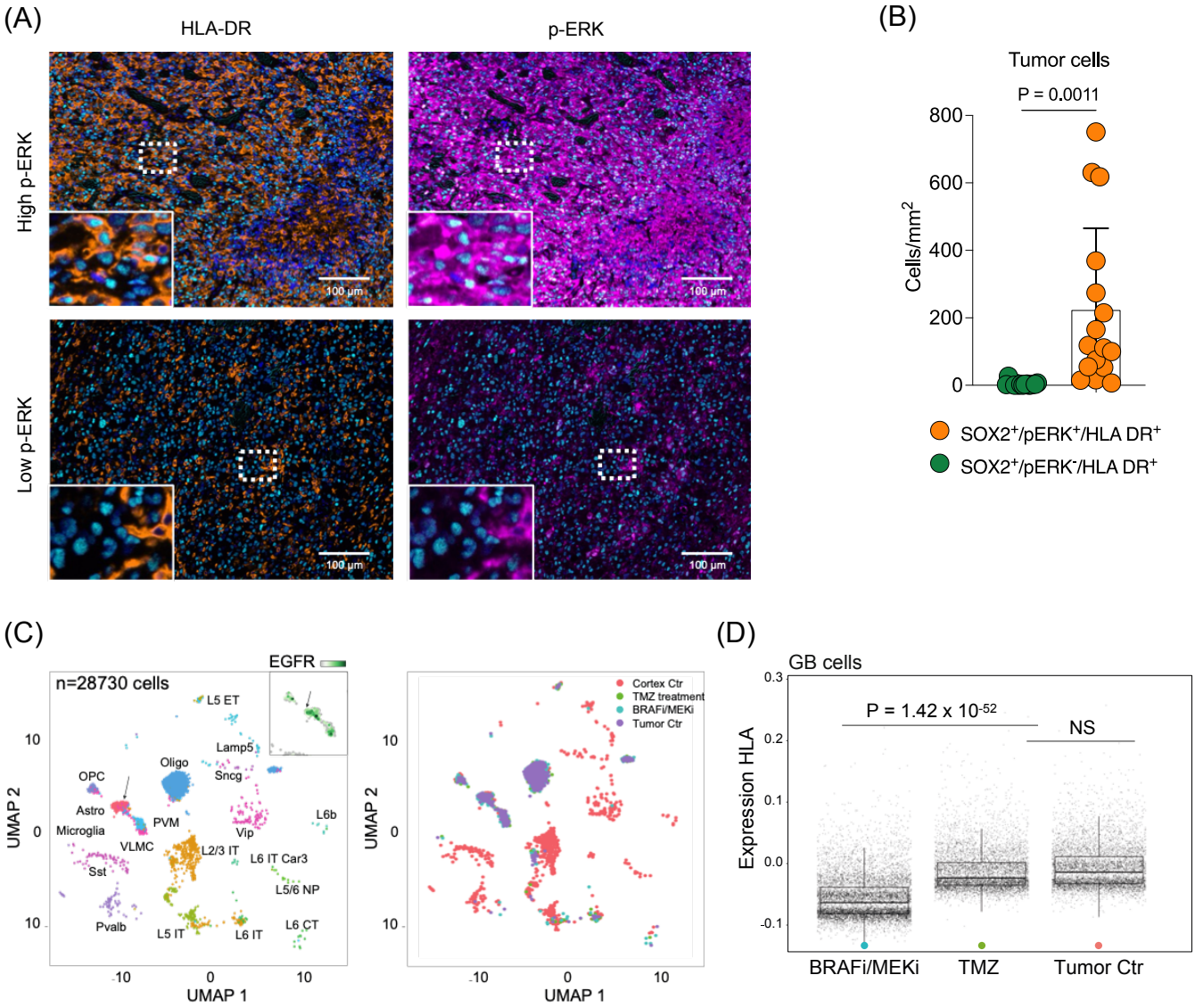
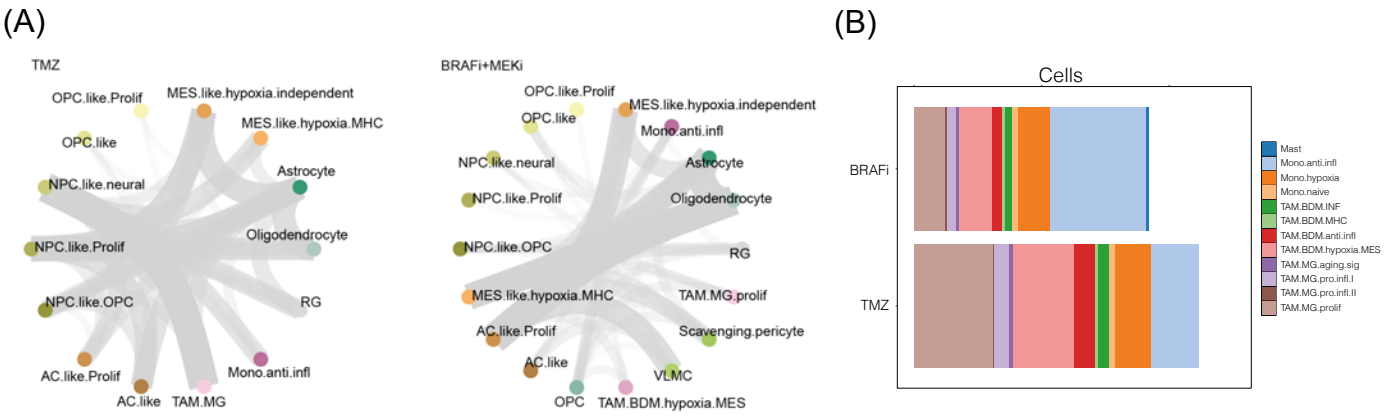
Figure 7. MAPK activation in GBM tumor is associated with interaction between tumor cell and microglia.